Supplementary Information for

Highly efficient photocatalytic degradation of dyes and anticancer activity of eco-friendly synthesized $Ag/Ag_2O/\gamma\text{-}Fe_2O_3$ nanoparticles using *Cistus monspeliensis* leaf extract

Radja Nada Boucetta[a,b*], Malika Khelfaoui[a,c], Nesrine Ammouchi[d], Sabrine Boucetta[e,f], Mohamed Nadir Khelifi[g], Erkan Can[h], Atmane Djermoune[i,j], Farid Ait Merzeg[i,j,k], Widad Sobhi[l], Faycal Djazi[b,d]

[a] *Department of Process Engineering, Faculty of Technology, 20 August 1955 University, El-Hadaeik Road, P.O. Box 26, Skikda 21000, Algeria*
[b] *Laboratoire de Recherche sur la Physico-Chimie des Surfaces et Interfaces (LRPCSI), 20 August 1955 University, El-Hadaeik Road, P.O. Box 26, Skikda 21000, Algeria*
[c] *Laboratory LGCES, Faculty of Technology, 20 August 1955 University, Skikda, 2100, Algeria*
[d] *Department of Sciences and Technology, Faculty of Technology, 20 August 1955 University, El-Hadaeik Road, P.O. Box 26, Skikda 21000, Algeria*
[e] *University 20 August 1955, Department of Nature and life sciences, Skikda, 21000, Algeria*
[f] *Laboratory of Ecobiology of Marine and Coastal Environments (EMMAL), Annaba University, 23000, Algeria*
[g] *Laboratoire de Génie des Procédés pour le Développement Durable et les Produits de Santé (LGPDDPS), Département Génie des Procédés, Ecole Nationale Polytechnique de Constantine, Algeria*
[h] Izmir Katip Celebi University, Faculty of Fisheries, Department of Aquaculture, Izmir, Türkiye
[i] *Scientific and Technical Research Center in Physical and Chemical Analysis (CRAPC), BP 384 Bou-Ismail, RP 42004 Tipaza, Algeria*
[j] *Research Unit in Physico-Chemical Analysis of Fluids and Soils (URAPC-FS), 11 Chemin Doudou Mokhtar, Ben Aknoun,16028 Alger, Algeria*
[k] *Technical Platform for Physico-chemical Analysis (PTAPC-Bejaia), Targa Ouzemmour, 06000 Bejaia, Algeria*
[l] *Biotechnology Research Center (CRBt), Nouvelle Ville Ali Mendjli UV03, Constantine 25000, Algeria*

**Corresponding author: Radja-Nada Boucetta , email : rn.boucetta@univ-skikda.dz*

This SI provides (i) XRD comparison of fresh vs stored batches (**Fig. S1**) and (ii) ROS scavenger tests with kinetics (**Fig. S2**).

i. XRD analysis of Fresh and Stored nanoparticles

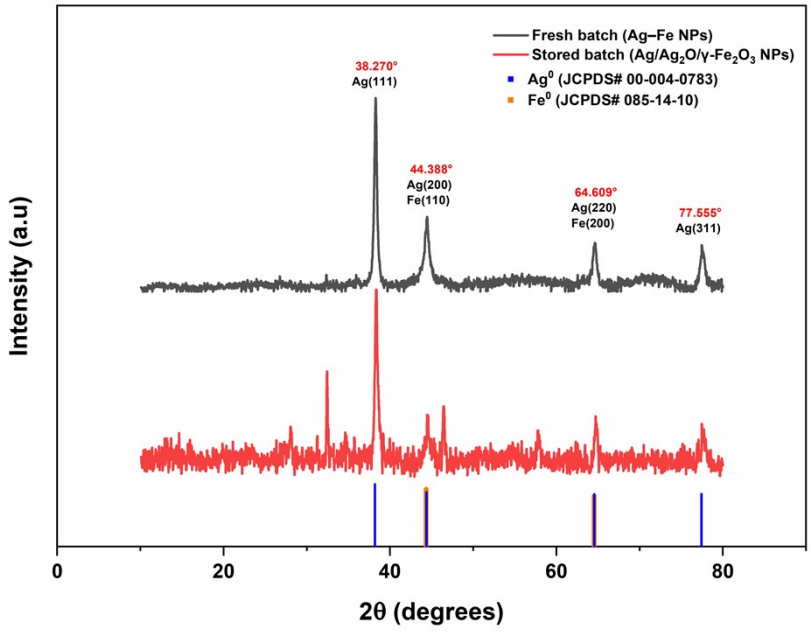

Fig. S1 XRD patterns of fresh and stored nanoparticles showing the effect of time on the structure.

Fig. S1 shows the XRD patterns of nanoparticles synthesized using Cistus monspeliensis aqueous extract, recorded shortly after synthesis (fresh, 2 days) and after storage. The stored sample was kept as a dried powder in a sealed 15 mL tube, protected from light, at 4 °C, and was periodically opened for analyses and applications. Therefore, storage was not under an inert atmosphere and may have allowed intermittent exposure to oxygen and humidity.

The fresh batch exhibits sharp peaks corresponding to metallic silver (Ag^0) at 2θ = 38.270°, 44.388°, 64.609°, and 77.555°, matching the (111), (200), (220), and (311) planes of the FCC structure of silver (JCPDS No. 00-004-0783). If an iron-containing phase is present, weak features at ~44.388° and ~64.609° could be consistent with the (110) and (200) planes of a BCC structure; however, these positions overlap with Ag reflections, and apparent Fe^0 contributions have been similarly interpreted in green Ag–Fe systems[1–3]. Thus, the presence of Fe^0 cannot be definitively confirmed without additional techniques like TEM or XPS. It is also possible that the iron oxides are too small (<3 nm) or amorphous to be detected by XRD[4].

After storage, the pattern shows clear phase evolution: reflections attributable to γ-Fe_2O_3 (maghemite) emerge at 26.42°, 27.88°, 32.33°, 35.69°, 57.73°, and 63.37°, consistent with γ-Fe_2O_3 (JCPDS No. 00-013-0458), alongside remaining Ag^0 and the appearance of Ag_2O peaks. Compared to the fresh batch, the stored sample displays an overall reduction in peak intensity, suggesting oxidation-related changes and possible decreases in crystallinity/partial amorphization associated with exposure to air and moisture during drying, storage, and repeated handling. Such behavior is expected because Fe^0 is unstable under oxygen- and water-containing environments and readily transforms to iron oxide phases; moreover, zero-valent iron nanoparticles commonly develop oxide/hydroxide surface layers even shortly after synthesis when exposed to air and water [5,6].

Overall, the XRD results indicate a transition from a fresh material dominated by crystalline Ag^0 (with possible overlapping Fe-related contributions) to a stored material where γ-Fe_2O_3 becomes evident and Ag oxidation products appear. This phase evolution is consistent with non-inert storage conditions and likely reflects oxidation and/or reduced crystallinity during storage and handling (intermittent exposure to air, humidity, and repeated opening of the tube). In addition, the initial drying step at 60 °C may not have fully removed residual water, and retained moisture could have further promoted oxidation and phase transformation during storage. A direct comparison of the fresh and stored batches is shown in **Fig. S1**.

ii. **Reactive Species Scavenging Tests for Crystal Violet Photocatalytic Degradation**

Following the protocol reported by S. Acharya et al.[7], the ROS scavenging tests were carried out to identify the dominant species involved in CV photocatalytic degradation. The experiments were performed using crystal violet (30 mg L^{-1}) with 0.1 g of the Ag/Ag_2O/γ-Fe_2O_3 nanoparticles, and the suspension was first kept in the

dark for 30 min to establish the adsorption–desorption equilibrium. After that, each scavenger (p-benzoquinone (BQ), Dimethyl Sulfoxide (DMSO), Isopropyl alcohol (IPA), and Disodium EDTA (EDTA)) was introduced using a 5 mM scavenger solution, where 20 mL was added to reach a final reaction volume of 200 mL, and the mixture was then exposed to UVA irradiation for 60 min under continuous stirring.

Fig. S2(a) shows the degradation profiles in the presence of each scavenger. A strong inhibition is clearly observed with BQ and DMSO, while EDTA causes only a minor reduction, and IPA leads to a slight enhancement. These trends are consistent with the pseudo-first-order (PFO) non-linear fitting results presented in **Fig. S2(b)**: the apparent rate constant (Kapp) decreases from 0.06465 min^{-1} (no scavenger, R^2 = 0.9783) to 0.00987 min^{-1} with DMSO (R^2 = 0.9445) and 0.00691 min^{-1} with BQ (R^2 = 0.7746), whereas EDTA gives 0.04676 min^{-1} (R^2 = 0.9642) and IPA slightly increases Kapp to 0.06888 min^{-1} (R^2 = 0.9834). The corresponding final removal efficiencies after 60 min are summarized in **Fig. S2(c)**, dropping from 92.47% (no scavenger) to 41.78% (DMSO) and 30.19% (BQ), while remaining high with EDTA (88.67%) and slightly increasing with IPA (94.95%). The lower R^2 observed for BQ likely reflects the strongly suppressed degradation (limited conversion), which can reduce the robustness of kinetic fitting.

Overall, the strong suppression by BQ supports that the electron–O_2 reduction route ($O_2^{\bullet-}$ formation) is central, since BQ is widely used to quench $O_2^{\bullet-}$ and/or intercept conduction-band electrons[8,9]. The pronounced inhibition with DMSO confirms a major contribution from •OH, as DMSO is a well-established •OH scavenger[10]. In contrast, the weak influence of EDTA suggests that direct h^+ oxidation is not the dominant pathway; moreover, scavenging h^+ does not necessarily eliminate •OH completely because •OH can still form through secondary routes (e.g., via $O_2^{\bullet-}$/H_2O_2). Finally, the slight enhancement with IPA can be explained by its sacrificial (electron-donor/hole-scavenging) role in some systems, which can reduce e^-/h^+ recombination and favor electron-driven O_2 reduction, sustaining ROS production[11,12]. Taken together, the scavenger trends support that CV degradation proceeds mainly through $O_2^{\bullet-}$ and •OH, with a secondary contribution from h^+.

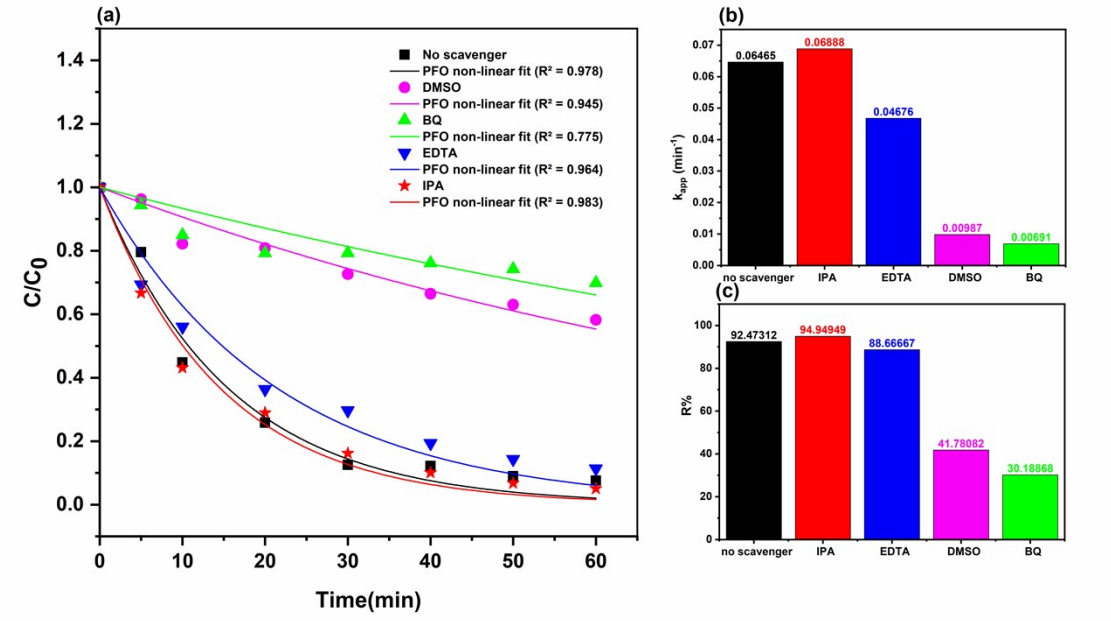

Fig. S2 Reactive species scavenging during UVA-driven photocatalytic degradation of crystal violet (CV) using $Ag/Ag_2O/\gamma\text{-}Fe_2O_3$ NPs: (a) degradation profiles in the presence of DMSO, BQ, EDTA, and IPA; (b) apparent rate constants (K_{app}) obtained from pseudo-first-order (PFO) non-linear fitting; (c) corresponding CV removal efficiencies after 60 min. *Experimental conditions: (C = 30 mg L^{-1}, pH = natural of the solution, V = 200ml, m = 0.1g, Light source = UVA, T= 20 ± 1 °C)*

References

1 M. R. Kamli, V. Srivastava, N. H. Hajrah, J. S. M. Sabir, A. Ali, M. A. Malik and A. Ahmad, *Antioxidants*, 2021, **10**, 182.

2 M. A. Malik, A. A. Alshehri and R. Patel, *Journal of Materials Research and Technology*, 2021, **12**, 455–470.

3 F. Murtaza, N. Akhter, M. A. Qamar, A. Yaqoob, A. A. Chaudhary, B. R. Patil, S. U.-D. Khan, N. A. Ibrahim, N. S. Basher, M. S. Aleissa, I. Kanwal and M. Imran, *Crystals*, 2024, **14**, 510.

4 S. Mourdikoudis, R. M. Pallares and N. T. K. Thanh, *Nanoscale*, 2018, **10**, 12871–12934.

5 D. O'Carroll, B. Sleep, M. Krol, H. Boparai and C. Kocur, *Advances in Water Resources*, 2013, **51**, 104–122.

6 T. Pasinszki and M. Krebsz, *Nanomaterials*, 2020, **10**, 917.

7 S. Acharya, S. Mansingh and K. M. Parida, *Inorg. Chem. Front.*, 2017, **4**, 1022–1032.

8 T. Liu, L. Wang, X. Lu, J. Fan, X. Cai, B. Gao, R. Miao, J. Wang and Y. Lv, *RSC Adv.*, 2017, **7**, 12292–12300.

9 J. Xiao, Y. Xie, Q. Han, H. Cao, Y. Wang, F. Nawaz and F. Duan, *Journal of Hazardous Materials*, 2016, **304**, 126–133.

10 E. Ouahiba, M. Chabani, A. A. Assadi, A. Abdeltif, F. Florence and B. Souad, *Res Chem Intermed*, 2023, **49**, 1–21.

11 V. Kumaravel, M. Imam, A. Badreldin, R. Chava, J. Do, M. Kang and A. Abdel-Wahab, *Catalysts*, 2019, **9**, 276.

12 S. Xu, K. Chen, Y. Cai, S. Ren, W. Chu, M. Song, Y. Xu and C. Tan, *Water Research*, 2025, **285**, 124139.